

TRANSFORMATION MECHANISMS AND INTERSTRATIFICATION IN CONVERSION OF SMECTITE TO KAOLINITE: AN HRTEM STUDY

MARC AMOURIC AND JUAN OLIVES

CRMC2-CNRS, Campus de Luminy, case 913, 13288 Marseille CEDEX 9, France

Abstract—The transformation of smectite into kaolinite and kaolinite–smectite interstratification were studied in samples belonging to the Argiles Plastiques formation of the Paris basin, by high-resolution transmission electron microscopy (HRTEM). Two original smectite phases, 1) beidellite with 1-nm-thick layers, and 2) beidellite–montmorillonite with 1.25-nm-thick layers, are progressively transformed into kaolinite–smectite mixed-layer minerals, and into kaolinite. As the percentage of kaolinite layers increases in the interlayered minerals, the kaolinite–smectite layer sequences, initially disordered, become locally more ordered, with the presence of KS and KKS units repeated 2 to 4 times (K = kaolinite layer, S = smectite layer). Two solid-state mechanisms seem to be responsible for the formation of kaolinite: 1) the transformation of 1 smectite layer into 1 kaolinite layer, denoted S→K, by stripping of a tetrahedral sheet and the adjacent interlayer region; 2) the intercalation of 1 kaolinite layer into smectite, denoted 0 (zero)→K. Structural and chemical incidences of these mechanisms are discussed.

Key Words—HRTEM, Interstratification, Kaolinite, Smectite, Transformation Mechanisms.

INTRODUCTION

Smectite, kaolinite and interlayered kaolinite–smectite are found in earth-surface conditions (soils, weathering profiles, etc.). Mixed-layer kaolinite–smectite was detected by X-ray diffraction (XRD) as randomly interstratified layers (Schultz et al. 1971; Wiewióra 1971; Wilson and Cradwick 1972; Triki et al. 1973; Thiry 1973), and as 1-1 ordered interstratification (that is, . . . KSKS . . . , where K and S denote a kaolinite and a smectite layer, respectively; Thomas 1989; Bertolino et al. 1991). Although direct observation of the individual layers and the interstratification sequences is possible with HRTEM (in the case of mixed-layer illite–smectite: Veblen et al. 1990; Jiang et al. 1990; Amouric and Olives 1991; Murakami et al. 1993; Olives and Amouric 1994), no such study exists for interlayered kaolinite–smectite, to our knowledge.

MATERIALS AND METHODS

In this paper (and in Olives and Amouric 1995), we present our first HRTEM and analytical electron microscopy (AEM) results on samples—supplied by M. Thiry—that come from the Early-Eocene Argiles Plastiques formation (Paris basin), in which the main clay minerals are smectite, mixed-layer kaolinite–smectite and kaolinite. These minerals were formed in tropical weathering profiles that developed at the end of Cretaceous time on preexisting rocks (mainly Cretaceous flint-bearing chalk), with a progressive evolution from smectite to interstratified kaolinite–smectite, and to kaolinite (Thiry et al. 1977). This is an especially significant sequence in that all intermediate stages of the smectite-to-kaolinite transformation can be found. The present study concerns 3 samples, in which mixed-layer kaolinite–smectite contains 10, 45 and 60% of

kaolinite layers, respectively (determined by XRD; Thiry 1991).

HRTEM experimental procedures are described in Amouric and Olives (1991) and Amouric et al. (1995). The samples, reduced to powders and embedded in Araldite resin, were sectioned with the diamond knife of an LKB ultramicrotome. The sections (less than 50 nm thick) were deposited on carbon-coated copper grids (by this technique, smectite layers are better preserved from dehydration than by ion-milling). Bright-field images were taken with a JEOL JEM-2000 FX electron microscope (200-kV accelerating voltage, 1.8-mm spherical aberration coefficient), with a 50- μ m objective aperture and at focus values in the range –100 to +100 nm. According to the literature (for example, Ahn and Peacor 1989; Veblen et al. 1990; Amouric and Olives 1991), it is very difficult to obtain high-quality HRTEM images of interstratified clays (white fringes will generally appear corrugated, vanishing in some parts and sometimes variable in thickness). This is particularly true for smectite–kaolinite mixtures, for which no HRTEM study has been described up to now. In addition, the minerals studied here have formed during a weathering-alteration process; they are thus rather badly crystallized and difficult to characterize. To minimize possible beam damage to the specimens, tilting procedures were therefore omitted. In addition, a low-light camera (LHESA EMLH 4086) equipped with an yttrium aluminium garnet (YAG) converter was systematically used under very low illumination. As a result, 1-dimensional images were mainly analyzed in this work. However, most of these showed characteristic 00 l lattice fringes of the mineral phases present in the samples. Simultaneously, AEM analyses were carried out on the same samples using

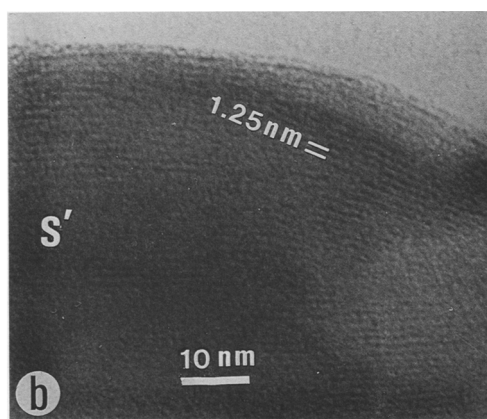
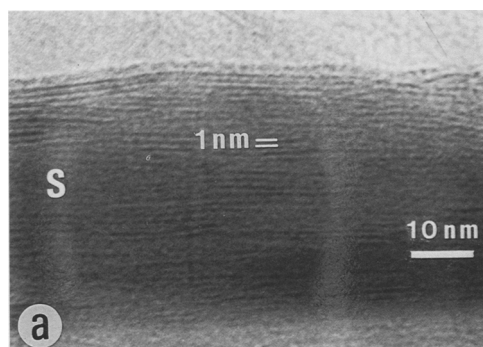


Figure 1. Lattice fringe images of a) an S type smectite crystal, with 1-nm-thick layers, and b) an S' type one, having 1.25-nm-thick layers.

a Tracor system (TN 5502) equipped with a Si(Li) detector. For good correlation between images and areas of chemical analyses, a beam probe 10 nm in diameter with constant beam current was used throughout the study (with a count time of 100 s). Collected data were processed by a program based on the method of Cliff and Lorimer (1975) and using appropriate layer silicate standards. In the structural formulas, all the iron was considered in Fe(III) state, as determined by Thiry (1991). Two octahedral cations per half cell were assumed (which implies that Mg cations may appear in the interlayer region).

RESULTS

Lattice-fringe spacings were generally measured between white fringes on the micrographs; however, HRTEM images of kaolinite single layers were specially difficult to obtain. Indeed, when individually observed in a stack, such layers may appear either as 0.7-nm-spaced fringes or as broad white fringes (with a narrow gray line sometimes visible in the middle) of 0.7-nm thickness. But kaolinite layers were often rec-

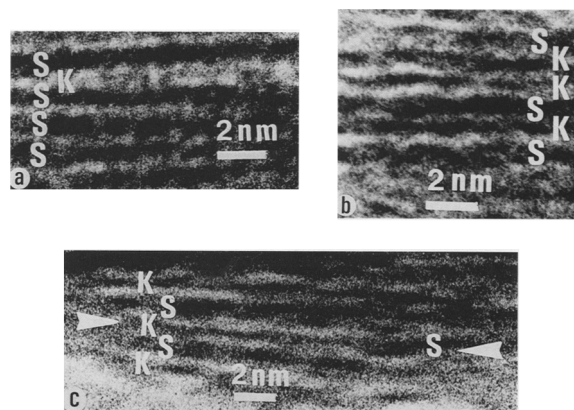
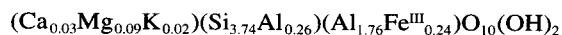


Figure 2. Lattice fringe images of various interstratified kaolinite-smectites of the 10%-kaolinite sample. S = S type smectite layer (1 nm thick). K = kaolinite layer (0.72 nm thick). In c), the lateral transition S→K is indicated by arrows.

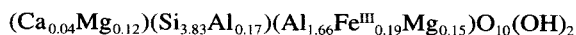
ognized as occurring in KS and KKS units, more or less periodically repeated in the stacks.

The 10%-Kaolinite Sample

In this sample, 2 types of smectite crystals were observed. The first type, denoted S, gives images showing only 1-nm fringe spacings (Figure 1a). In the other type, denoted S', the fringes are 1.25-nm regularly spaced (Figure 1b). AEM chemical analyses (15 to 20 analyses for each species) show that S crystals have a composition corresponding to the mean formula:



while that for S' crystals is:



(in these formulas, standard deviations are 0.06 for Si and Al, 0.05 for Mg and Fe, and 0.02 for Ca and K). In this sample, the 1-nm smectite crystals are more abundant than the 1.25-nm ones.

In addition to these smectite crystals, we also observed mixed-layer kaolinite-smectite. The kaolinite-smectite layer sequences are disordered, as illustrated in Figure 2. The interstratified smectite fringes are mainly 1 nm thick, and then interpreted to be of the S type. Although rare, some 1.25-nm smectite fringes (S' type) have been also observed. Finally, lateral transitions of 1 S smectite layer into 1 kaolinite layer are visible in images of the same specimen (Figure 2c). Such transitions are denoted S→K.

The 45%-Kaolinite Sample

In this sample, we observed interlayered kaolinite-smectite containing both S and S' layers, in similar proportions (Figure 3). The S fringes are dominant and the S' ones rare in some areas (as in Figures 3a and 3b), or vice versa in others. Large fringe spacings of

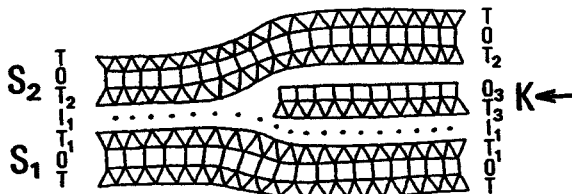


Figure 5. Intercalation of a kaolinite layer K between 2 smectite layers S_1 and S_2 . View parallel to the layers. T, O and I respectively denote the tetrahedral, octahedral and interlayer levels. Some of them are marked with indices, for the discussion. In the right side of the figure, a double structure is probably present: $T_1I_1T_3$ structure of smectite type, and $T_3O_3T_2$ of kaolinite type.

ations mentioned above. With our assumption of 2 octahedral cations per half cell, these formulas represent a beidellite (or beidellite–nontronite) composition for S, and a beidellite–montmorillonite intermediate composition (with also a nontronite component) for S' . The S and S' smectite crystals thus being identified as 2 probable distinct phases, we have then interpreted 1-nm smectite layers to be of the S type and 1.25-nm ones of the S' type, in all the studied samples and the observed interlayered sequences.

In contrast with the disordered kaolinite–smectite layer sequences of the 10%-kaolinite sample, the observed repetition of KS, KS' and KKS units indicates some degree of local order in interlayered kaolinite–smectite of the 45%-kaolinite sample: R1 or first-neighbor order type for KS and KS' ; R2 or second-neighbor order type for KKS. A higher degree of local order is present in the 60%-kaolinite sample, as indicated by the larger proportion of KS' units (R1 order), the presence of KKS' units (R2 order) and the greater number of repeated units.

Mechanisms

The above HRTEM observations of the lateral transitions S (or S')→K and 0→K indicate 2 possible solid-state mechanisms that are responsible for kaolinite formation: 1) the lateral transformation of 1 smectite layer into 1 kaolinite layer (S→K or S' →K); 2) the lateral intercalation of 1 kaolinite layer in smectite (0→K). As usual in phyllosilicates, the term “solid-state” is here considered in a wide sense, since the preceding transitions obviously imply mass transports. It merely indicates that these mechanisms occur within the solid, at a cell scale (at the front of the new developing layer, the reaction being probably facilitated by the presence of water) and preserve the major part of the preexisting solid. The 1 layer→1 layer solid-state transformation has been reported in various cases: 1 biotite layer→1 chlorite layer, equivalent to 1 interlayer K plane→1 brucite-like layer (Olives et al. 1983; Olives and Amouric 1984; Olives 1985; Maresch et al. 1985), 1 biotite layer→1 brucite-like layer

(equivalent to 2 biotite layers→1 chlorite layer; Veblen and Ferry 1983; Eggleton and Banfield 1985), 1 smectite layer→1 illite layer (Amouric and Olives 1991; Murakami et al. 1993), or 1 serpentine layer→1 illite layer (Amouric et al. 1995). Note that the mechanism S→K (or S' →K), observed in our 3 samples, produces a decrease in volume, whereas the mechanism 0→K (observed in the 60%-kaolinite sample) implies an increase in volume.

Structural Incidence

In mechanism 0→K, a kaolinite layer K is intercalated between 2 smectite layers S_1 and S_2 , that is, between the interlayer atoms and the tetrahedral level of a smectite layer (Figure 5). These interlayer atoms are preserved, since no diminution of layer thickness has been observed (indeed, the removal of the interlayer water molecules would reduce the thickness of an S' layer from 1.25 to 1 nm, and that of a KS' unit from 2 to 1.75 nm).

In order to compare this 0→K mechanism with the S (or S')→K one, it will be useful to determine what structural defect is produced by each mechanism. In addition to the shift that is normal to the layers (due to the increase or decrease in volume), such a defect generally involves a shift parallel to the layers. In the following, we try to estimate this “additional basal shift”, for the 0→K mechanism. Let S_1S_2 denote the basal shift between S_1 and S_2 (that is, that between the centers of hexagons of tetrahedra T_1 and those of T_2 ; Figure 5), S_1KS_2 the basal shift between the same levels T_1 and T_2 when K is intercalated between S_1 and S_2 , S_1K the basal shift between T_1 and T_3 , and KS_2 that between T_3 and T_2 . The intercalation of K might then produce an additional basal shift between S_1 and S_2 (that is, a difference of basal shifts between the right side and the left side of Figure 5), given by:

$$\begin{aligned} S_1KS_2 \text{ (right side)} - S_1S_2 \text{ (left side)} \\ = (S_1K + KS_2) - S_1S_2 \\ \approx S_1K - \frac{a_K}{3} - S_1S_2 \end{aligned} \quad [1]$$

a_K being defined in Figure 6. Note that, if the interlayer shift S_1K can be an arbitrary vector of the basal plane (as it occurs in smectite turbostratic stacking), its value would probably be such that the additional basal shift—written above—vanishes, in order to minimize the elastic distortion between S_1 and S_2 . But this is not the only possible case, and an additional basal shift may subsist.

In the other mechanism, S (or S')→K, the main structural modification probably involves the removal (or stripping) of a tetrahedral sheet and the adjacent interlayer region (Figure 7). As above, let S_1S_2 denote the basal shift between T'_1 and T_2 (Figure 7), S_1 that

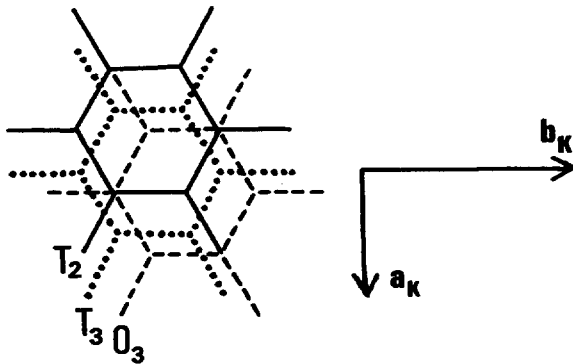


Figure 6. Kaolinite structure of the $T_3O_3T_2$ stacking of Figure 5. View normal to the layers, from top to bottom of Figure 5. The hexagonal networks of the cations of the successive levels T_3 , O_3 and T_2 are respectively represented by dotted, dashed and solid lines. The symbols a_K and b_K are the usual basal cell vectors of kaolinite (here limited to the $T_3O_3T_2$ structure).

between T_1 and T'_1 , and KS_2 that between T_1 and T_2 (for the KS_2 stacking). As in the preceding case, this transformation $S \rightarrow K$ would generally produce an additional basal shift between T_1 and T_2 , given by:

KS_2 (right side of Figure 7) - ($S_1 + S_1S_2$) (left side)

$$\begin{aligned} &\approx -\frac{a_K}{3} - \left(-\frac{a_S}{3} + S_1S_2\right) \\ &\approx -\frac{a_K}{6} + \frac{b_K}{6} - S_1S_2 \\ &\approx \frac{a_S}{6} + \frac{b_S}{6} - S_1S_2 \end{aligned} \quad [2]$$

where a_K , b_K , a_S , b_S are defined in Figure 8, the vectors (a_K , b_K) being rotated by 60° from (a_S , b_S), that is, $a_K = a_S/2 - b_S/2$, $b_K = 3a_S/2 + b_S/2$ (assuming the transoctahedral sites vacant in S_1). Note that this additional basal shift is generally not equal to 0 , except if the interlayer shift S_1S_2 has the particular value $a_S/6 + b_S/6$.

Thus, the 2 preceding mechanisms produce a bending of the layers (associated with the increase or the decrease in volume), and an additional basal shift, which may vanish in some cases. According to the nature of interlayer atoms, it seems probable that the S' smectite stacking is mainly turbostratic (absence of K, presence of H_2O), while the S smectite one is mainly semi-random (presence of K, absence of H_2O). With such an assumption, the $0 \rightarrow K$ mechanism would be easier in S' smectite than in S smectite, since the additional basal shift vanishes only in the former case (as discussed above). This is consistent with our observations: the $0 \rightarrow K$ mechanism is only present in the S' -rich sample, that is, the 60%-kaolinite one. In order to compare the S (or S') $\rightarrow K$ and $0 \rightarrow K$ mechanisms, complementary chemical considerations are needed.

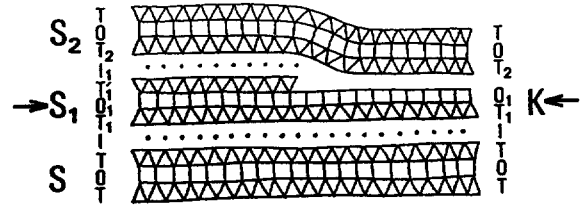


Figure 7. Transformation of 1 smectite layer (S_1) into 1 kaolinite layer (K). View parallel to the layers. Same notations as in Figure 5. Some layers and levels are distinguished by indices or primes, for the discussion. In the right side of the figure, the $T_1O_1T_2$ structure is probably of kaolinite type.

Chemical Aspects

In the S (or S') $\rightarrow K$ mechanism, a tetrahedral sheet and the adjacent interlayer region are removed (Figure 7). In addition, the remaining tetrahedral and octahedral sheets of the smectite layer (T_1 and O_1 in Figure 7) are slightly modified, Al being replaced by Si in the tetrahedral sheet and, in the octahedral sheet, Fe and Mg being replaced by Al, and H being added to the outer oxygens. The corresponding global chemical reaction would be:

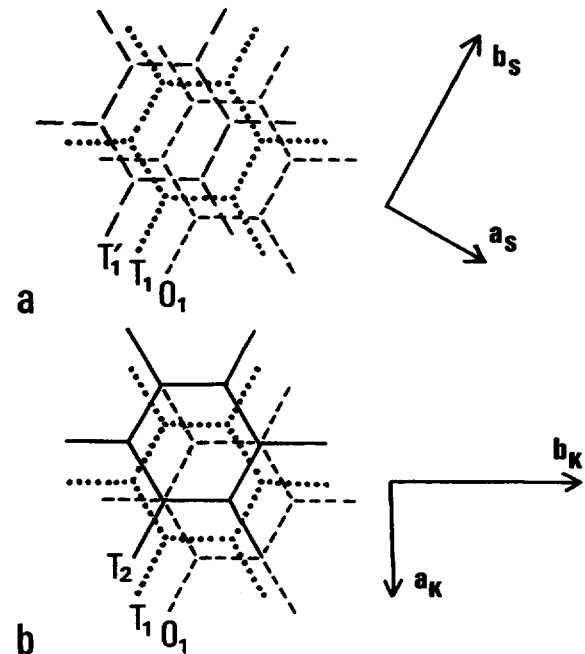
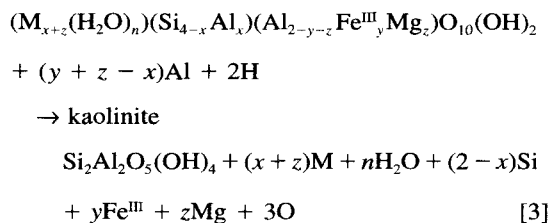
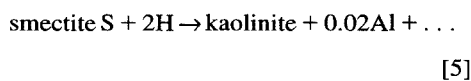
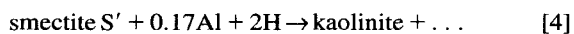


Figure 8. Stacking structures of the levels T'_1 and T_2 above T_1O_1 , with the notations of Figure 7. Views normal to the layers, from top to bottom of Figure 7. The hexagonal networks of the cations of the levels T_1 , O_1 , T'_1 and T_2 are respectively represented by dotted, short-dashed, long-dashed and solid lines. a) $T_1O_1T'_1$ stacking in the smectite layer S_1 (with transoctahedral sites vacant). The symbols a_S and b_S are the usual basal cell vectors referred to the 1 layer S_1 . b) $T_2O_1T_1$ stacking with kaolinite structure (KS_2 region). The symbols a_K and b_K are the usual basal cell vectors of kaolinite (here limited to the $T_2O_1T_1$ structure).

smectite



in which M = Na, K, Mg_{0.5}, Ca_{0.5} (note that $y + z - x$ may be positive or negative). In the present case, almost no supply of atoms is needed to perform the transformations. Indeed, only 0.17Al + 2H have to be added to S' and only 2H to S, the respective reactions being:



Note that, no Al being supplied to S in the preceding reaction, the S→K transformation might be easier than the S'→K one.

On the contrary, in the other mechanism 0→K, all the atoms necessary to create the new kaolinite layer must be provided (possibly from some dissolution of surrounding smectite). From this chemical point of view, the S (or S')→K mechanism would seem preferable to the 0→K one.

Comparison of the Mechanisms

In the less-kaolinitized samples, S smectite layers are dominant. The 2 mechanisms S→K and 0→K seem structurally equivalent, as both may produce an additional basal shift (see above). Nevertheless, the easier one is probably S→K, since very few atoms have to be supplied in this case. Our observations support this interpretation: the 0→K mechanism was not observed in the 10%- and 45%-kaolinite samples.

By comparing the 3 samples, we also observed that the relative abundance of the S' smectite layers with respect to the S ones increases as the percentage of kaolinite layers increases. This variation may be explained by the above inference that the S→K mechanism is probably easier than the S'→K one.

By this process, the remaining smectite layers are mainly of S' type, in the more-kaolinitized sample (60%-kaolinite). The 2 mechanisms S'→K and 0→K are then present, the former being favored from chemical arguments (few atoms supplied) and the latter from structural ones (no additional basal shift), as discussed above. These 2 mechanisms compensate each other, 0→K producing an increase in volume and S'→K a decrease in volume.

CONCLUSIONS

HRTEM images of mixed-layer kaolinite-smectite have been obtained for the first time, to our knowledge.

In the studied samples, 2 original smectite phases are progressively transformed into interlayered kaolinite-smectite, and into kaolinite. The kaolinite-smectite layer sequences are disordered in the less-kaolinitized samples, and present an increasing local order, as the percentage of kaolinite layers increases (this is very similar to the case of interstratified illite-smectite; Amouric and Olives 1991; Olives and Amouric 1994). Such an order is characterized by the repetition (a few times) of KS units (R1 order) and KKS ones (R2 order).

Two solid-state mechanisms (in the wide meaning of the expression) seem to be responsible for the formation of kaolinite: 1) the transformation of 1 smectite layer into 1 kaolinite layer, denoted S→K, by stripping of a tetrahedral sheet and the adjacent interlayer region; 2) the intercalation of 1 kaolinite layer into smectite, denoted 0 (zero)→K. The structural and chemical changes produced by these mechanisms are discussed in detail. It is shown that such specific changes may favor one mechanism or the other.

ACKNOWLEDGMENTS

The authors would like to thank M. Thiry for providing the samples observed in this study.

REFERENCES

- Ahn JH, Peacor DR. 1989. Illite/smectite from Gulf Coast shales: A reappraisal of transmission electron microscope images. *Clays Clay Miner* 37:542-546.
- Amouric M, Olives J. 1991. Illitization of smectite as seen by high-resolution transmission electron microscopy. *Eur J Mineral* 3:831-835.
- Amouric M, Parron C, Casalini L, Giresse P. 1995. A (1:1) 7-Å Fe phase and its transformation in recent sediments: An HRTEM and AEM study. *Clays Clay Miner* 43:446-454.
- Bertolino SRA, Murray HH, Depetris PJ. 1991. Regular kaolinite/smectite (R1) from the Bermejo river basin, Argentina. *Clays Clay Miner* 39:658-660.
- Cliff G, Lorimer GW. 1975. The quantitative analysis of thin specimens. *J Microscopy* 103:203-207.
- Eggleton RA, Banfield JF. 1985. The alteration of granitic biotite to chlorite. *Am Mineral* 70:902-910.
- Jiang WT, Peacor DR, Merriman RJ, Roberts B. 1990. Transmission and analytical electron microscopic study of mixed-layer illite/smectite formed as an apparent replacement product of diagenetic illite. *Clays Clay Miner* 38:449-468.
- Maresch WV, Massone HJ, Czank M. 1985. Ordered and disordered chlorite/biotite interstratifications as alteration products of chlorite. *N Jb Miner* 152:79-100.
- Murakami T, Sato T, Watanabe T. 1993. Microstructure of interstratified illite/smectite at 123 K: A new method for HRTEM examination. *Am Mineral* 78:465-468.
- Olives J. 1985. Biotites and chlorites as interlayered biotite-chlorite crystals. *Bull Mineral* 108:635-641.

- Olives J, Amouric M. 1984. Biotite chloritization by interlayer brucitization as seen by HRTEM. *Am Mineral* 69:869–871.
- Olives J, Amouric M. 1994. Transformation of smectite into illite and illite–smectite interstratification: HRTEM observations and lattice energies calculations. *Electron Microscopy vol 2B, ICEM 13-Paris: Les Editions de Physique*. p 1281–1282.
- Olives J, Amouric M. 1995. HRTEM study of the transformation of smectite into kaolinite. *Terra Nova* 7, Abstract Suppl 1:252–253.
- Olives J, Amouric M, de Fouquet C, Baronnet A. 1983. Interlayering and interlayer slip in biotite as seen by HRTEM. *Am Mineral* 68:754–758.
- Schultz LG, Shepard AO, Blackmon PD, Starkey HC. 1971. Mixed-layer kaolinite–montmorillonite from the Yucatan Peninsula, Mexico. *Clays Clay Miner* 19:137–150.
- Thiry M. 1973. Les sédiments de l'éocène inférieur du Bassin de Paris et leurs relations avec la paléooaltération de la craie [thèse 3e cycle]. Strasbourg. 79 p.
- Thiry M. 1991. Les argiles plastiques du bassin de Paris. Fontainebleau: Ecole des Mines, Livret guide d'excursion, Réunion du Groupe Français des Argiles. 47 p.
- Thiry M, Cavelier C, Trauth N. 1977. Les sédiments de l'éocène inférieur du bassin de Paris et leurs relations avec la paléooaltération de la craie. *Sci Géol Bull* 30:113–128.
- Thomas AR. 1989. A new mixed layer clay mineral. Regular 1:1 mixed layer kaolinite/smectite. *Abstr Annu Meet Clay Miner Soc; Sacramento, California*. 69.
- Triki R, Thiry M, Trauth N, Eberhart JP. 1973. Mise en évidence d'interstratifiés de type kaolinite-montmorillonite dans une argile du bassin de Paris. *C R Acad Sci Paris D* 276:881–884.
- Veblen DR, Ferry JM. 1983. A TEM study of the biotite–chlorite reaction and comparison with petrologic observations. *Am Mineral* 68:1160–1168.
- Veblen DR, Guthrie GD, Livi KJT, Reynolds RC. 1990. High-resolution transmission electron microscopy and electron diffraction of mixed-layer illite/smectite: Experimental results. *Clays Clay Miner* 38:1–13.
- Wiewióra A. 1971. A mixed-layer kaolinite–smectite from Lower Silesia, Poland. *Clays Clay Miner* 19:415–416.
- Wilson MJ, Cradwick PD. 1972. Occurrence of interstratified kaolinite/montmorillonite in some Scottish soils. *Clay Miner* 9:425–437.

(Received 9 January 1997; accepted 23 January 1998; Ms. 97-006)